Multivalent GU-rich oligonucleotides sequester TDP-43 in the nucleus by inducing high molecular weight RNP complexes

Xi Zhang[1], Tanuza Das[1], Petr Kalab[2*], Lindsey R. Hayes[1,3*]

[1]Johns Hopkins School of Medicine Department of Neurology, [2]Johns Hopkins University Whiting School of Engineering, [3]Johns Hopkins School of Medicine Brain Science Institute

*Correspondence to: petr@jhu.edu, lhayes@jhmi.edu

ABSTRACT

The loss of nuclear TDP-43 localization and its accumulation in cytoplasmic aggregates are hallmarks of neurodegeneration and major therapeutic targets. We recently demonstrated that TDP-43 binding to endogenous nuclear GU-rich RNAs sequesters TDP-43 in the nucleus and restricts its passive nuclear export. Here, we tested the feasibility of synthetic RNA oligonucleotide-mediated augmentation of TDP-43 nuclear localization. Using biochemical assays, we compared the ability of GU-rich oligonucleotides to engage in multivalent, RRM-dependent binding with TDP-43 and identified (GU)16 as a strong multivalent binder. When transfected into cells, unlike monovalent oligonucleotides that displaced TDP-43 from the nucleus, (GU)16 preserved steady-state TDP-43 nuclear localization and prevented transcriptional blockade-induced TDP-43 mislocalization. RNA pulldowns from (GU)16-transfected cells confirmed that (GU)16 induced high molecular weight RNP complexes, incorporating TDP-43 and possibly other GU-binding proteins. Transfected (GU)16 caused partial failure of TDP-43 cryptic exon repression, likely because the high-affinity oligonucleotides diverted TDP-43 from endogenous RNAs. Thus, while GU-rich oligonucleotides can attenuate TDP-43 mislocalization, optimization is needed to avoid TDP-43 loss of function.

INTRODUCTION

TDP-43 is an essential nucleic-acid binding protein that regulates RNA splicing and stability.[1] Like other heterogeneous nuclear ribonucleoproteins (hnRNPs), TDP-43 shuttles between the nucleus and cytoplasm and is predominantly nuclear in healthy cells.[2,3] In 'TDP-43 proteinopathies', a class of neurodegenerative disorders that includes amyotrophic lateral sclerosis (ALS), frontotemporal dementia (FTD), limbic-predominant age-related TDP-43 encephalopathy (LATE), and related disorders, affected cells in the central nervous system show TDP-43 nuclear clearance and cytoplasmic aggregation.[4] Though TDP-43 mutations have been identified in rare genetic cases,[5] most patients with TDP-43 proteinopathy have sporadic, non-inherited disease. Despite advances in understanding the regulation of TDP-43 nucleocytoplasmic transport and the downstream consequences of TDP-43 mislocalization,[6] the molecular events initiating TDP-43 mislocalization in neurodegeneration remain obscure. The development of therapies targeting TDP-43 nuclear clearance, loss of function, and cytoplasmic aggregation is of major interest toward slowing the progression of neurodegeneration.[7]

TDP-43 is a 43-kDa protein with an N-terminal oligomerization domain followed by a nuclear localization sequence (NLS), tandem RNA recognition motifs (RRM1 and RRM2), and a C-terminal intrinsically disordered region that mediates liquid-liquid phase separation (LLPS).[8] Structural analysis demonstrates that the RNA binding groove of RRM1-2 contacts 10 nucleotides of a 5′-GNGUGNNUGN-3′ motif, with 'AUG12' (5'-GUGUGAAUGAAU-3') binding TDP-43 stably in a single conformation.[9] Crosslinking immunoprecipitation (CLIPseq) from cell lines, mouse, and postmortem human brain confirms that TDP-43 binds GU- and GUA-rich RNA motifs primarily within introns, as well as a subset of noncoding RNAs, miRNAs, and mRNAs.[10–12] Notably, TDP-43 binds its own 3'-UTR at a sequence termed Clip34nt to autoregulate its expression.[10,13] Binding up to one-third of the mammalian transcriptome, TDP-43 functions prolifically in the regulation of RNA processing, including alternative splicing,[10,11] the repression of cryptic exons,[12] alternative polyadenylation,[14] miRNA processing,[15] and long interspersed nuclear elements (LINEs).[16]

The nucleocytoplasmic localization of TDP-43 is regulated by a dynamic balance between nuclear import and export. The active nuclear import of TDP-43 primarily occurs via NLS binding to importins α and β, although

passive import also likely occurs as evidenced by modest nuclear entry of TDP-43-ΔNLS.[2,17] The nuclear export of full-length TDP-43, initially thought to occur via exportin-1 (XPO1) binding to a putative nuclear export signal (NES) in the RRM2 domain, was subsequently shown to occur by passive diffusion through nuclear pore channels and is exquisitely size-dependent.[18–21] In multiple export assays, the addition of bulky tags markedly delayed TDP-43 nuclear export by raising its size above the permeability barrier of the nuclear pore complex (NPC), which increasingly excludes cargoes above 30-60 kDa in size.[22] An exception is the short TDP-43 isoform, which is upregulated by pathologic hyperexcitability and localizes to the cytoplasm via a distinct NES for XPO1 arising in the C-terminus.[23]

We recently demonstrated that the nuclear localization of full-length TDP-43 critically depends on binding to nuclear RNAs, which sequester TDP-43 in the nucleus and restrict its availability for passive nuclear export.[21] In permeabilized and live cell nuclear export assays, depletion of nuclear RNA binding sites for TDP-43, via RNase degradation or inhibition of transcription, released TDP-43 for passive diffusion from the nucleus. RRM mutations or displacement of TDP-43 from endogenous nuclear RNAs with monovalent (GU)6 oligonucleotides also promoted cytoplasmic mislocalization. Conversely, inhibiting splicing to promote the accumulation of nuclear intronic binding sites for TDP-43 promoted TDP-43 nuclear retention. Based on these data, we hypothesized that longer exogenous GU-rich oligonucleotides might augment TDP-43 nuclear localization, provided the oligonucleotides form multivalent complexes with TDP-43 large enough to restrict its diffusion through the NPC.

Here, we report the characterization and functional outcome of GU-rich oligonucleotides tested for their ability to promote TDP-43 nuclear retention. The TDP-43 binding valency of candidate oligonucleotides with ≥2 predicted TDP-43 binding sites, of differing lengths and sequences, was tested in biochemical assays and living cells. (GU)16 robustly induced TDP-43 RRM1,2 multimerization *in vitro* and promoted the formation of heterogenous, high molecular weight TDP-43 complexes in living cells. Remarkably, (GU)16 prevented TDP-43 mislocalization following transcriptional blockade, confirming that exogenous oligonucleotides can scaffold TDP-43 and promote its nuclear retention. However, transfected (GU)16 impaired TDP-43 function in cryptic exon repression, indicating that optimization of the exogenous GU-RNAs is needed to promote TDP-43 nuclear localization without compromising its function.

RESULTS

Multivalent interactions of GU-rich oligonucleotides with TDP-43

GU-rich oligonucleotide sequences were selected with well-characterized TDP-43 binding motifs and the established or predicted ability to form multimers with TDP-43 (**fig 1a**). The multivalent binding of TDP-43 to GU-rich RNAs is well demonstrated. Endogenous TDP-43 RNA binding sites frequently occur in clusters that coordinate multivalent binding depending on sequence, length, and density.[24] Biochemical assays confirm that the valency of TDP-43 binding to synthetic oligonucleotides is length-dependent, with monovalent binding ≤(GU)6 and multivalent binding ≥(GU)12.[25] Pure GU-repeats and the 'AUG12' motif exhibit low nanomolar affinity (0.8-26.9 nM) for TDP-43 in *in vitro* assays,[9,26–28] while Clip34nt affinity has been estimated at 97-520 nM.[27,29] Clip34nt is a 34-base G, U, and A-rich sequence that strongly promotes TDP-43 LLPS[26] and has shown promise as a chaperone to disaggregate cytoplasmic TDP-43.[30] The Clip34nt binding valency for TDP-43 has not yet been established.

(GU)16, ('AUG12')2, and Clip34nt oligonucleotides were synthesized with 2'-O-methyl and PS-modifications commonly utilized to stabilize antisense oligonucleotides (ASO) against RNase degradation[31] and binding to recombinant SUMO-tagged RRM1,2 was analyzed. First, electrophoretic mobility shift assays (EMSAs) were performed by combining each oligonucleotide with increasing concentrations of RRM1,2 and RNA-protein complexes were resolved by native electrophoresis (**fig 1b-c**). All three GU-rich oligonucleotides readily bound RRM1,2. A32 and (CA)16 were utilized as controls for specificity, and no appreciable binding with RRM1,2 was observed. As previously reported,[25] (GU)6 showed a single band shift with increasing RRM1,2 concentrations, indicating one binding event. ('AUG12')2, Clip34nt, and (GU)16 all exhibited multiple, discrete band shifts with increasing protein concentrations, suggesting multimers. Quantifying band shifts likely to involve more than two RRM1,2 molecules showed that (GU)16 had the highest propensity for multivalency, followed by Clip34nt (**fig 1c**). >2 binding events were rarely observed for ('AUG12')2. To determine the molecular weight of the RNA-protein complexes, the amine-crosslinker bis(sulfosuccinimidyl)suberate (BS3) was utilized before SDS-PAGE and proteins were visualized with silver stain (**fig 1d**). As predicted from the EMSAs, (GU)6 formed monomers,

(‘AUG12’)2 formed a mix of monomers and dimers, and Clip34nt and (GU)16 additionally formed ~120-130 kDa complexes, likely corresponding to tetramers. The putative tetrameric complexes appeared most abundant with (GU)16 although silver stain is poorly quantitative.

Binding valency predicts the effect of GU-rich oligonucleotides on TDP-43 nuclear localization

Previously, we showed that (GU)6 rapidly entered transfected HeLa cell nuclei, bound TDP-43, and promoted nuclear efflux, likely by competitive displacement of TDP-43 from endogenous nuclear RNAs, freeing the resulting ~45 kD complex for passive diffusion through nuclear pore channels.[21] Since (GU)6 exclusively forms monovalent complexes with TDP-43 **(fig 1b-c**), next we tested multivalent GU-oligonucleotides. A 3’-biotin label was utilized to enable oligonucleotide visualization and biochemical analysis. 5 h post-transfection, cells were fixed and labeled with fluorescently tagged streptavidin (SAV). (‘AUG12’)2-bio, Clip34nt-bio, and (GU)16-bio readily entered transfected cells (**fig 2a**). The N/C partitioning of the oligonucleotides differed, with (‘AUG12’)2 showing nuclear enrichment and Clip34nt and (GU)16-bio showing more equivalent nuclear and cytoplasmic signal (**fig 2b**). In addition to diffuse signal, all three oligonucleotides showed scattered puncta predominantly in the cytoplasm suggesting a tendency to demix and self-associate. TDP-43 immunolabeling demonstrated that (‘AUG12’)2, which showed the lowest propensity for multivalent binding, elicited dose-dependent TDP-43 nuclear exit (**fig 2c-d**), reminiscent of (GU)6.[21] Clip34nt elicited modest nuclear exit. In contrast, (GU)16 did not alter the steady-state localization of TDP-43. Thus, the tendency of GU-rich oligonucleotides to elicit TDP-43 nuclear efflux inversely correlated with TDP-43 binding valency.

(GU)16 prevents transcriptional blockade-induced TDP-43 mislocalization

Since (GU)16 showed the highest potential for multivalent TDP-43 interactions (**fig 1**) and did not induce TDP-43 nuclear efflux (**fig 2**), we predicted that the size of nuclear (GU)16-TDP-43 complexes may exceed the passive diffusion limits of nuclear pore channels. To test that hypothesis, (GU)16-transfected cells were treated with the RNA Pol II inhibitor NVP2 to block transcription and deplete the nucleus of TDP-43 binding sites within nascent pre-mRNAs. As we previously reported,[21] NVP2 rapidly induced TDP-43 cytoplasmic mislocalization in untransfected cells (**fig 3a-c**). Remarkably, NVP2-induced TDP-43 mislocalization was attenuated in (GU)16-transfected cells in a dose-dependent manner. At 62.5 nM (GU)16, NVP2-induced TDP-43 nuclear efflux was

completely abolished. Specifically, (GU)16 attenuated the decrease in nuclear intensity and increase in cytoplasmic intensity induced by NVP2, confirming the blockade of TDP-43 translocation to the cytoplasm (**fig 3c**). In contrast, NVP2-induced TDP-43 cytoplasmic mislocalization was essentially unaltered in Clip34nt, ('AUG12')2, and (CA)16-transfected cells (**fig 3d-f**).

(GU)16 induces the formation of heterogeneous high molecular weight RNP complexes

Next, we tested if transfected (GU)16 oligomers induce high molecular weight RNP complexes in cells, consistent with our biochemical data (**fig 1**) and the predicted mechanism of TDP-43 nuclear retention by multivalent binding. HeLa cells were transfected with biotinylated (GU)6 or (GU)16, alongside polyA or CA-repeat oligonucleotides of equal lengths. After 5 h, transfected cells were UV-irradiated to form covalent RNA-protein complexes and analyzed by SAV RNA-pulldowns (**fig 4a**). Only trace TDP-43 binding to polyA or CA-repeat oligonucleotides was observed. As we previously reported, in (GU)6-transfected cells, SAV precipitated predominantly 43-45 kDa TDP-43 monomers,[21] whereas in (GU)16-transfected cells, SAV-precipitated numerous higher molecular weight bands that were not multiples of 43 kD. Thus, (GU)16 may induce the formation of heterogeneous TDP-43-containing RNP complexes that incorporate other nuclear proteins via direct (GU)16 binding. Immunolabeling for other nuclear RNA binding proteins (RBPs) in (GU)16 transfected cells showed that the localization of MATR3, FUS, and hnRNPL at steady-state and after NVP2 treatment were unaffected by (GU)16 (**fig 4 d-f**). However, (GU)16 partially attenuated the NVP2-induced nuclear efflux of hnRNPA1 and hnRNPA2/B1 (**fig 4b-c**). Neither hnRNPA1 nor hnRNPA2/B1 are predicted to bind GU-rich motifs,[32,33] but both have been shown to interact with TDP-43[34] suggesting that the (GU)16 response may be mediated by protein-protein interactions. Consistent with this, hnRNPA1 and hnRNPA2/B1 were not identified as direct (GU)16 binders in the SAV RNA-pulldowns, nor other RBPs, including MATR3, ELAVL1, ELAVL3, hnRNPC, SNRPA, or PSF (**suppl fig 1**). FUS exhibited modest binding to (GU)16, which is not expected from its consensus motif (CAGGACAGCCAG),[35] and hnRNPL bound (CA)16, consistent with its preferred binding to CA-repeat motifs.[36] No other direct RNA binding was observed.

(GU)16-induced TDP-43 nuclear retention is RRM1,2-dependent

While effective in promoting RNase resistance, PS modification of RNA oligonucleotides has also been shown to increase protein binding.[37] To verify that (GU)16-induced TDP-43 nuclear retention is mediated by specific binding to the TDP-43 RRM domains, we generated stable, monoclonal HeLa cell lines expressing V5-tagged wild-type TDP-43 ($TDP43^{WT}$-V5) or TDP-43 containing five point mutations in the RRM1-2 domains that abolish RNA binding ($TDP43^{5FL}$-V5)[38] (**fig 5a**). As we previously reported, the steady-state N/C ratio of $TDP43^{5FL}$-V5 was reduced compared to $TDP43^{WT}$-V5 and $TDP43^{5FL}$-V5 showed no NVP2-induced nuclear efflux.[21] Next, the cell lines were transfected with (GU)16 for 5 h followed by NVP2 transcriptional blockade, and the localization of V5-tagged TDP-43 was analyzed by immunofluorescence (**fig 5b-d**). Like endogenous TDP-43 (**fig 3**), (GU)16 inhibited NVP2-induced $TDP43^{WT}$-V5 mislocalization in a dose-dependent manner **(fig 5b**). However, (GU)16 had no effect on the localization of $TDP43^{5FL}$-V5 **(fig 5c**). Comparison of the NVP2-induced TDP-43 nuclear exit in WT vs 5FL-transfected cells showed that (GU)16 only altered the localization of $TDP43^{WT}$-V5 (**fig 5d**), consistent with the notion that (GU)16 alters TDP-43 localization via specific binding to the RRM1,2 domain.

To further validate the direct (GU)16 interaction with RRM1-2, we performed SAV pulldowns from oligo-transfected $TDP43^{WT}$-V5 or $TDP43^{5FL}$-V5 cell lines (**fig 5e**). Immunoblots of the pulldowns developed with V5 antibodies (**fig 5e, left)** showed that transfection with (GU)6 and (GU)16 induced high molecular weight $TDP43^{WT}$-V5 crosslinks, whose pattern was virtually identical to the crosslinks with endogenous TDP-43 (**fig 5e, right**), except for the small increase in size resulting from the 1.4kDa V5 tag. A barely detectable interaction of $TDP43^{5FL}$-V5 with (GU)16 was noted (**fig 5e, left**). $TDP43^{WT}$-V5 but not $TDP43^{5FL}$-V5 showed low-level binding to (CA)16). As previously demonstrated, $TDP43^{WT}$-V5 but not $TDP43^{5FL}$-V5 downregulated endogenous TDP-43 expression via autoregulation (**fig 5e, inset**).[29] These data confirm that (GU)16 regulates TDP-43 localization by specific direct binding to the RRM1-2 domains.

(GU)16 causes partial TDP-43 loss of function

GU-rich oligonucleotides exhibit low nanomolar affinity for TDP-43[9,26–29] and PS modification increases oligonucleotide protein binding.[37] We suspected that although (GU)16 preserves steady-state TDP-43 nuclear localization (**fig 2-3)**, high-affinity binding of PS-protected (GU)16 to TDP-43 may divert TDP-43 from endogenous RNAs and disrupt TDP-43 splicing regulatory function. To test this, we analyzed TDP-43 cryptic exon repression in EPB41L4A, a TDP-43-regulated transcript in both HeLa cells[12,39] and iPSC-derived

neurons[40] (**fig 6**). To assess EPB41L4A sensitivity as a TDP-43 functional readout, we generated samples in which TDP-43 protein was depleted by approximately 50% (24 h post-siRNA transfection), versus cells in which TDP-43 was fully depleted by CRISPR (**fig 6a).**[41] RT-PCR confirmed that EPB41L4A cryptic exon inclusion is detectable even after 50% loss of TDP-43 protein (**fig 6b**). Cells transfected with (CA)16 for 6, 18, or 24h showed no EPB41L4A cryptic exon inclusion, in contrast to (GU)16-transfected cells where the EPB41L4A cryptic exon was detectable by 6h and increased by 18h. Since the expression of EPB41L4A mRNA decreases with TDP-43 knockdown,[12] we designed a qRT-PCR assay to quantify EPB41L4A cryptic exon incorporation normalized to EPB41L4A mRNA levels (**fig 6c**). qRT-PCR confirmed that (GU)16 transfection increases the EPB41L4A cryptic exon to mRNA ratio, commensurate with a partial loss of TDP-43 splicing regulatory function.

DISCUSSION

We recently reported that TDP-43 is sequestered in the nucleus of healthy cells by binding to endogenous nuclear GU-rich RNAs, thus restricting its passive nuclear efflux.[21] In those studies, we found that competitive displacement of TDP-43 from endogenous nuclear RNAs by monovalent (GU)6 freed TDP-43 for passive diffusion from the nucleus. We hypothesized that the loss of nuclear GU-RNA enrichment may contribute to TDP-43 mislocalization in neurodegeneration. While the state of the nucleocytoplasmic GU-RNA gradient in disease remains to be examined, we sought to test the capacity of exogenous RNA oligonucleotides to augment TDP-43 nuclear localization. Here, we report that exogenous, multivalent (GU)16 oligonucleotides sequester TDP-43 within the nucleus by forming high molecular weight RNP complexes that exceed the passive limits of the NPC. Transfection with low nanomolar (GU)16 concentrations preserved TDP-43 nuclear localization following transcriptional blockade-induced depletion of nuclear TDP-43 pre-mRNA binding sites. Together, these data strongly support a model of RNA-based nuclear sequestration of TDP-43 (**fig 6d**) and suggest that RNA-based therapeutics may be a useful strategy to attenuate TDP-43 mislocalization, provided that the loss of TDP-43 function can be avoided.

The dose-dependent response of TDP-43 localization to (GU)16 (**fig 3**) suggests that, for an RNA-based approach to be effective in regulating RBP localization, the intracellular concentration of the exogenous RNA needs to reach a critical level, perhaps approaching the concentration of the target protein. Our results indicate

that lipid-mediated transfection of synthetic RNA oligonucleotides, in principle, meets such a requirement to acutely preserve TDP-43 localization. Among the synthetic RNA oligonucleotides we tested, the formation of multimeric RRM1,2 complexes in EMSAs correlated with TDP-43 nuclear retention upon transfection into cells. A combination of multiple factors likely determined the overall effect on TDP-43 localization, including valency toward TDP-43 versus other RBPs sharing a similar motif preference, the nucleocytoplasmic localization of the oligonucleotides, and effects on TDP-43 LLPS.[26] Like (GU)16, Clip34nt showed a propensity to engage in multivalent binding with purified RRM1,2 and was similarly distributed throughout the cell, but did not attenuate transcriptional blockade-induced nuclear efflux. Interestingly, Clip34nt exhibits lower affinity for TDP-43 than pure GU-repeat oligonucleotides in biochemical assays.[27,29] Clip34nt is also predicted to form a hairpin structure, compared to (GU)16 or ('AUG12')2, which are unstructured. The potential effect of RNA secondary structure on TDP-43-RNA binding is yet unexplored.

(GU)16 transfection caused partial TDP-43 loss of function despite promoting TDP-43 nuclear retention (**fig 6**). For an exogenous RNA-based approach to have therapeutic potential, the function of TDP-43 must be preserved. To meet such a requirement, the exogenous RNA must possess optimal binding activity towards TDP-43, thus precluding competitive displacement of TDP-43 from essential pre-mRNA targets. The design of optimally modified bases could be informed by progress in ASOs and related oligonucleotide therapeutics.[31,42] Alternatively, systematic screens to tune the expression levels and affinity of native GU-RNAs expressed from exogenous vectors could lead to an effective RNA-based TDP-43 targeting strategy. Previous studies showed that RNA motifs containing pure GU repeats differ in their ability to promote TDP-43 phase transition compared to GU intermixed with A and C, indicating that the optimization of either synthetic or endogenously expressed RNAs should involve screens for optimal RNA motifs.[24,43] In addition, exogenous TDP-43-binding RNAs have also been shown to oppose pathologic TDP-43 demixing and aggregation in biochemical assays and living cells.[28,30] An ideal RNA-based intervention for TDP-43 proteinopathies would combine both nuclear localization and disaggregation properties.

METHODS

Cell lines

A single cell-derived HeLa cell clone was maintained in OptiMEM (Gibco/ThermoFisher) with 4% FBS and grown at 37° in humidified air containing 5% CO2. Monoclonal cell lines stably expressing V5-tagged wild-type or RRM-mutant TDP-43 were generated by transient transfection using puromycin selection followed by limiting dilution cloning (for plasmids, see **suppl table 1b**). A monoclonal TDP-43 CRISPR-knockout HeLa cell line was generously provided by Shawn Ferguson[41] and maintained in DMEM (Gibco/ThermoFisher) with 10% FBS. Cells were frequently refreshed from frozen stocks validated by STR profiling (ATCC) and verified to be mycoplasma negative (Genlantis).

Oligonucleotides

Synthetic RNA oligonucleotides were obtained from IDT. Sequences and modifications are listed in **suppl table 1a**. Desalted lyophilized oligonucleotides were reconstituted in sterile, RNAse- and DNAse-free water and single-use aliquots were stored at -80°C.

Oligonucleotide transfections

24 h prior to transfection, HeLa cells were plated on optical glass-bottom 96-well plates (CellVis) at 10,000 cells per well, or in 6-well plates at 300,000 cells per well. As previously described,[21] synthetic oligonucleotides were transfected using Lipofectamine RNAiMax (ThermoFisher). RNA oligomers were diluted in Opti-MEM and mixed 1:1 with diluted lipofectamine (1.5-3 µL per 25 µL Opti-MEM). After a 5 min incubation at room temperature, transfection mixes were added to culture media at 10-30 µL transfection mix per 100 µL media in 96-well plates or scaled proportionally for 6-well plates. The lipofectamine concentration and volume per well were individually optimized utilizing biotinylated versions of each oligonucleotide sequence to maximize dose-dependent nuclear entry, via SAV-647 labeling. The oligonucleotide concentrations shown represent the final concentration following dilution in culture media. Mock transfection controls were treated with RNAiMAX alone. For transcriptional inhibition, cells were treated with 250 nM NVP2 for 90 min (Tocris Bioscience). At the time points indicated in the figure legends, cells were fixed in 4% paraformaldehyde/PBS (Electron Microscopy Sciences) for 15 min.

Immunofluorescence

Paraformaldehyde-fixed cells were rinsed once with PBS and then blocked and permeabilized with 10% normal goat serum (NGS, Vector Labs) and 0.1% Triton-X-100 in PBS for 15-30 min at room temperature. Primary antibodies (**suppl table 1c**) were applied for 1 h at room temperature or overnight at 4°C in 10% NGS/PBS. Following two PBS rinses, AlexaFluor-labeled secondary antibodies (ThermoFisher) were applied for 1 h at room temperature in 5% NGS/PBS. To visualize biotinylated oligomers, streptavidin-AF647 (ThermoFisher) was added together with secondary antibody at 1:500. Cells were rinsed with PBS containing Hoechst 33342 and stored in 50% glycerol/PBS until imaging.

RNA extraction and RT-PCR

Cells were rinsed in PBS and lysed in TRIzol (ThermoFisher). Total RNA was isolated using the miRNeasy kit (Qiagen) following the manufacturer's protocol with DNase digestion. cDNA synthesis was performed with the Iscript cDNA synthesis kit (Bio-Rad). RT-PCR for gel electrophoresis (primers listed in **suppl table 1d**) was performed using Platinum II Hot-Start Green PCR Master Mix (ThermoFisher), and products separated on 2% EX e-gels containing SYBR Gold II (Invitrogen). qRT-PCR using custom TaqMan primers/probes was performed with TaqMan Fast Advanced Master Mix on a QuantStudio 3 Real-Time PCR System.

RRM1-2 cloning and recombinant protein production

The RRM1-2 domain of human TDP-43, including amino acids 102-269, was PCR-amplified from wt-TDP43-tdTomato-HA plasmid (Addgene 28205, a gift from Zuoshang Xu)[44] and cloned in frame with the N-terminal 6-His-SUMO-TEV-site into the SspI site of pET 6His-SUMO-TEV LIC (1S) (Addgene 29659, a gift from Scott Gradia) using the HiFi Assembly kit (NEB). NEBuilder Assembly Tool 2.0 was used to design RRM1-2 primers with 21-bp overlap with the destination vector. The correct sequence of the resulting pET 6His-SUMO-TEV-RRM1-2 plasmid was verified by restriction digests and Sanger sequencing.

6His-SUMO-RRM1-2 protein production was performed in BL21-DE3 *E. coli* cells (Thermo), using LB media with 50µg/ml Kanamycin. Cells transformed with the pET 6His-SUMO-TEV-RRM1-2 plasmid were plated on an LB-agar plate and grown at 37ºC overnight. The next day, a 250 mL starter culture was initiated with a single large colony and grown overnight on a shaker at 30ºC, reaching OD_{600nm} =~1.4. 100 mL of the starter was

added to 1L media in 2.8L Fehrnbach baffle-free flask and incubated at 30ºC, 225 rpm for 3.5 h, reaching OD_{600nm} =~0.4. The culture was supplemented with 0.3mM IPTG and incubated at 30ºC, 100 rpm for 3.5 h before cell harvesting and washing with 10mM imidazole in PBS (pH7.4), freezing in liquid nitrogen, and storage at -80ºC. Protein purification started by quickly thawing the cells in ~15 mL room-temperature 10mM imidazole with protease inhibitor cocktail (Roche) and freshly added 200µM PMSF. Cells were lysed by sonication on ice and lysates were clarified at 26500G, 40 min, 4ºC. The clarified lysate was incubated on a rotator (50 min, 4ºC) with 1 mL (packed volume) HIS-Select HF Nickel Affinity Gel (Sigma). The beads were collected in 15 mL Poly-Prep chromatography column (Bio-Rad) and washed with 15 mL 10mM imidazole before stepwise elution with 3ml each of PBS, pH7.4 containing increasing Imidazole concentrations (25-1000mM). Aliquots of the eluates were separated on a 4-20% SDS-PAGE gel, and peak fractions (corresponding to 50-150mM imidazole) were identified by Coomassie staining. Pooled peak fractions were dialyzed overnight in PBS, clarified at 21000G, 4ºC, 3 min, and protein concentration was measured before aliquoting, snap-freezing in liquid nitrogen and storage at -80ºC.

EMSAs

Oligonucleotides were diluted to 10 pmol in binding buffer (20 mM HEPES, pH 7.6 containing 25 mM KCl, 1 mM TCEP, and 2 mM $MgCl_2$).[25] A serial dilution of SUMO-RRM1,2 protein (0-40 pmol) was prepared, mixed 1:1 with oligonucleotide, and incubated at room temperature for 1 h. Samples were diluted in 5X TBE running buffer (Invitrogen/ThermoFisher) and run on 10% polyacrylamide gels (Invitrogen/ThermoFisher) at 200 V for 45 min on ice in pre-chilled 1X Ultrapure TBE Buffer (Fisher Scientific). Gels were rinsed in 1X TBE and immersed in SYBR Gold nucleic acid gel stain (1:10,000) (Invitrogen/ThermoFisher) for 30 min prior to fluorescent imaging on an ImageQuant LAS 4000 gel imaging system (GE). Band density was quantified using ImageJ.

Biotinylated RNA-pulldowns

HeLa cells were transfected as described above in 6-well plates and crosslinked for RNA pulldowns as previously described.[21] Briefly, 5 h post-transfection, cells were rinsed with DPBS and UV crosslinked (λ=254 nm, 1.5 J/cm^2 on ice) before harvesting by trypsinization. Cells were washed twice with DPBS, resuspended in lysis buffer (1% NP40 in PBS, pH 7.4 with protease inhibitor cocktail (Roche), and 2.5% v/v RNase inhibitor),

and sonicated 10s on ice. After clarification of the lysates by centrifugation (21,000g, 5 min, 4°C) and protein concentration measurement, samples were diluted with lysis buffer to equal concentration (2-4 µg/µL). An equal total protein amount of lysate per sample was then added to DPBS-washed magnetic SAV-conjugated beads (Thermo-Fisher MyOneC1, ~1 µL beads/ 15-20µg sample) and rotated at 4°C for 1.5 h. Beads were collected on a magnetic stand, supernatants removed and beads washed 5 times with ice-cold RIPA buffer (10mM Tris-HCl, pH 8.0, 5mM EDTA,1% Triton X-100, 0.5% Sodium Deoxycholate, 0.1% SDS, 150mM NaCl), transferred to the new set of tubes, rinsed twice with water and resuspended in 20 µL Laemmli sample buffer (Bio-Rad, 2X with 5% β-mercaptoethanol). After boiling for 5 min at 100°C, tubes were briefly centrifuged, placed on a magnetic stand, and the eluates separated by SDS-PAGE, along with aliquots of inputs prepared in Laemmli sample buffer. After transfer to PVDF membranes, immunoblots were blocked for 30-60 min with 5% non-fat dried milk (Biorad) in TTBS (0.05% Tween-20, TBS, pH7.4) and incubated overnight at 4°C with primary antibodies. After incubation with horseradish peroxidase-coupled secondary antibodies (20 min, room temperature) and washes with TTBS, ECL images were photographed using ImageQuant LAS400.

Microscopy and automated image analysis

Automated cell imaging was performed on an ImageXpress Micro Confocal high content microscope (Molecular Devices) as previously described.[21,45] HeLa cells were imaged with 20x objective in spinning disc confocal mode with 60 µM pinhole at sub-saturating exposures. A 3 x 3 grid of nine non-overlapping images were routinely collected from each well yielding an average of approximately 2000 cells per well. Background-corrected mean nuclear and cytoplasmic intensities and the nuclear/cytoplasmic (N/C ratio) were analyzed using the MetaXpress software translocation-enhanced module (Molecular Devices). All image analysis was performed on raw, unaltered images and uniformly filtered to exclude errors of cell identification (probe intensity = 0) or non-physiologic results (N/C ratio <0.1 or >100). High resolution images of oligonucleotide localization were obtained using an LSM980 confocal microscope (Zeiss) with a 63x oil objective.

Image processing for figures

Minimal processing was done using Adobe Photoshop 2023, limited to cropping and maximizing the intensity histogram according to the dimmest and brightest pixels in each image. In selected figures, the ‘fire’ pseudo-

color look-up-table (LUT/ImageJ) was applied to aid in data visualization. The quantitative, linear LUT map is provided in those images. All adjustments were linear (no gamma changes) and applied equally to the entire image. Immunoblots and gels were cropped for space and the intensity histogram was maximized according to the dimmest and brightest pixels. Uncropped gel images are shown in **suppl fig 2**.

Statistical analysis

Curve fitting and statistical analyses were performed using Prism software (Graphpad). Oligonucleotide dose-response curves were fit by simple linear or non-linear regression analysis. Differences among groups were analyzed by ANOVA with post-hoc tests for multiple comparisons. The number of biological replicates (independent cell passages and experiments) was used as the N for all analyses.

REFERENCES

1. Prasad A, Bharathi V, Sivalingam V, Girdhar A, Patel BK. Molecular Mechanisms of TDP-43 Misfolding and Pathology in Amyotrophic Lateral Sclerosis. Frontiers in molecular neuroscience. 2019;12:25.

2. Ayala YM, Zago P, D'Ambrogio A, Xu YF, Petrucelli L, Buratti E, Baralle FE. Structural determinants of the cellular localization and shuttling of TDP-43. J Cell Sci. 2008 Nov 15;121(Pt 22):3778–85.

3. Dreyfuss G, Kim VN, Kataoka N. Messenger-RNA-binding proteins and the messages they carry. Nature reviews Molecular cell biology. 2002 Mar;3(3):195–205.

4. Boer EMJ de, Orie VK, Williams T, Baker MR, Oliveira HMD, Polvikoski T, Silsby M, Menon P, Bos M van den, Halliday GM, Berg LH van den, Bosch LVD, Damme P van, Kiernan MC, Es MA van, Vucic S. TDP-43 proteinopathies: a new wave of neurodegenerative diseases. J Neurology Neurosurg Psychiatry. 2021;92(1):86–95.

5. Buratti E. Functional Significance of TDP-43 Mutations in Disease. Adv Genet. 2015;91:1–53.

6. Tziortzouda P, Bosch LVD, Hirth F. Triad of TDP43 control in neurodegeneration: autoregulation, localization and aggregation. Nat Rev Neurosci. 2021;22(4):197–208.

7. Hayes LR, Kalab P. Emerging Therapies and Novel Targets for TDP-43 Proteinopathy in ALS/FTD. Neurotherapeutics. 2022;19(4):1061–84.

8. François-Moutal L, Perez-Miller S, Scott DD, Miranda VG, Mollasalehi N, Khanna M. Structural Insights Into TDP-43 and Effects of Post-translational Modifications. Frontiers in molecular neuroscience. 2019;12:1199.

9. Lukavsky PJ, Daujotyte D, Tollervey JR, Ule J, Stuani C, Buratti E, Baralle FE, Damberger FF, Allain FHT. Molecular basis of UG-rich RNA recognition by the human splicing factor TDP-43. Nature Structural & Molecular Biology. 2013 Dec;20(12):1443–9.

10. Polymenidou M, Lagier-Tourenne C, Hutt KR, Huelga SC, Moran J, Liang TY, Ling SC, Sun E, Wancewicz E, Mazur C, Kordasiewicz H, Sedaghat Y, Donohue JP, Shiue L, Bennett CF, Yeo GW, Cleveland DW. Long pre-mRNA depletion and RNA missplicing contribute to neuronal vulnerability from loss of TDP-43. Nature Neuroscience. 2011 Apr;14(4):459–68.

11. Tollervey JR, Curk T, Rogelj B, Briese M, Cereda M, Kayikci M, König J, Hortobágyi T, Nishimura AL, Zupunski V, Patani R, Chandran S, Rot G, Zupan B, Shaw CE, Ule J. Characterizing the RNA targets and position-dependent splicing regulation by TDP-43. Nature Neuroscience. 2011 Apr 1;14(4):452–8.

12. Ling JP, Pletnikova O, Troncoso JC, Wong PC. TDP-43 repression of nonconserved cryptic exons is compromised in ALS-FTD. Science. 2015 Aug 7;349(6248):650–5.

13. Ayala YM, Conti LD, Avendaño-Vázquez SE, Dhir A, Romano M, D'Ambrogio A, Tollervey J, Ule J, Baralle M, Buratti E, Baralle FE. TDP-43 regulates its mRNA levels through a negative feedback loop. The EMBO Journal. 2011 Jan 19;30(2):277–88.

14. Melamed Z, López-Erauskin J, Baughn MW, Zhang O, Drenner K, Sun Y, Freyermuth F, McMahon MA, Beccari MS, Artates JW, Ohkubo T, Rodriguez M, Lin N, Wu D, Bennett CF, Rigo F, Cruz SD, Ravits J, Lagier-Tourenne C, Cleveland DW. Premature polyadenylation-mediated loss of stathmin-2 is a hallmark of TDP-43-dependent neurodegeneration. Nature Neuroscience. 2019 Feb;22(2):180–90.

15. Kawahara Y, Mieda-Sato A. TDP-43 promotes microRNA biogenesis as a component of the Drosha and Dicer complexes. Proc National Acad Sci. 2012;109(9):3347–52.

16. Liu EY, Russ J, Cali CP, Phan JM, Amlie-Wolf A, Lee EB. Loss of Nuclear TDP-43 Is Associated with Decondensation of LINE Retrotransposons. Cell Reports. 2019 Apr 30;27(5):1409-1421.e6.

17. Winton MJ, Igaz LM, Wong MM, Kwong LK, Trojanowski JQ, Lee VMY. Disturbance of nuclear and cytoplasmic TAR DNA-binding protein (TDP-43) induces disease-like redistribution, sequestration, and aggregate formation. The Journal of biological chemistry. 2008 May 9;283(19):13302–9.

18. Pinarbasi ES, Cağatay T, Fung HYJ, Li YC, Chook YM, Thomas PJ. Active nuclear import and passive nuclear export are the primary determinants of TDP-43 localization. Scientific reports. 2018 May 4;8(1):7083.

19. Ederle H, Funk C, Abou-Ajram C, Hutten S, Funk EBE, Kehlenbach RH, Bailer SM, Dormann D. Nuclear egress of TDP-43 and FUS occurs independently of Exportin-1/CRM1. Scientific reports. 2018 May 4;8(1):7084.

20. Archbold HC, Jackson KL, Arora A, Weskamp K, Tank EMH, Li X, Miguez R, Dayton RD, Tamir S, Klein RL, Barmada SJ. TDP43 nuclear export and neurodegeneration in models of amyotrophic lateral sclerosis and frontotemporal dementia. Scientific reports. 2018 Mar 15;8(1):4606.

21. Duan L, Zaepfel BL, Aksenova V, Dasso M, Rothstein JD, Kalab P, Hayes LR. Nuclear RNA binding regulates TDP-43 nuclear localization and passive nuclear export. Cell Reports. 2022;40(3):111106.

22. Timney BL, Raveh B, Mironska R, Trivedi JM, Kim SJ, Russel D, Wente SR, Sali A, Rout MP. Simple rules for passive diffusion through the nuclear pore complex. The Journal of Cell Biology. 2016 Oct 10;215(1):57–76.

23. Weskamp K, Tank EM, Miguez R, McBride JP, Gómez NB, White M, Lin Z, Gonzalez CM, Serio A, Sreedharan J, Barmada SJ. Shortened TDP43 isoforms upregulated by neuronal hyperactivity drive TDP43 pathology in ALS. Journal of Clinical Investigation. 2020 Mar 2;130(3):1139–55.

24. Hallegger M, Chakrabarti AM, Lee FCY, Lee BL, Amalietti AG, Odeh HM, Copley KE, Rubien JD, Portz B, Kuret K, Huppertz I, Rau F, Patani R, Fawzi NL, Shorter J, Luscombe NM, Ule J. TDP-43 condensation properties specify its RNA-binding and regulatory repertoire. Cell. 2021;184(18):4680-4696.e22.

25. Rengifo-Gonzalez JC, Hage KE, Clément MJ, Steiner E, Joshi V, Craveur P, Durand D, Pastré D, Bouhss A. The cooperative binding of TDP-43 to GU-rich RNA repeats antagonizes TDP-43 aggregation. Elife. 2021;10:e67605.

26. Grese ZR, Bastos AC, Mamede LD, French RL, Miller TM, Ayala YM. Specific RNA interactions promote TDP-43 multivalent phase separation and maintain liquid properties. Embo Rep. 2021;22(12):e53632.

27. Bhardwaj A, Myers MP, Buratti E, Baralle FE. Characterizing TDP-43 interaction with its RNA targets. Nucleic acids research. 2013 May;41(9):5062–74.

28. French RL, Grese ZR, Aligireddy H, Dhavale DD, Reeb AN, Kedia N, Kotzbauer PT, Bieschke J, Ayala YM. Detection of TAR DNA-binding protein 43 (TDP-43) oligomers as initial intermediate species during aggregate formation. Journal of Biological Chemistry. 2019 Apr 26;294(17):6696–709.

29. Koehler LC, Grese ZR, Bastos ACS, Mamede LD, Heyduk T, Ayala YM. TDP-43 Oligomerization and Phase Separation Properties Are Necessary for Autoregulation. Front Neurosci-switz. 2022;16:818655.

30. Mann JR, Gleixner AM, Mauna JC, Gomes E, DeChellis-Marks MR, Needham PG, Copley KE, Hurtle B, Portz B, Pyles NJ, Guo L, Calder CB, Wills ZP, Pandey UB, Kofler JK, Brodsky JL, Thathiah A, Shorter J, Donnelly CJ. RNA Binding Antagonizes Neurotoxic Phase Transitions of TDP-43. Neuron. 2019 Apr 17;102(2):321-338.e8.

31. Khvorova A, Watts JK. The chemical evolution of oligonucleotide therapies of clinical utility. Nat Biotechnol. 2017;35(3):238–48.

32. Wu B, Su S, Patil DP, Liu H, Gan J, Jaffrey SR, Ma J. Molecular basis for the specific and multivariant recognitions of RNA substrates by human hnRNP A2/B1. Nat Commun. 2018;9(1):420.

33. Jain N, Lin HC, Morgan CE, Harris ME, Tolbert BS. Rules of RNA specificity of hnRNP A1 revealed by global and quantitative analysis of its affinity distribution. Proceedings of the National Academy of Sciences. 2017 Feb 28;114(9):2206–11.

34. Freibaum BD, Chitta RK, High AA, Taylor JP. Global analysis of TDP-43 interacting proteins reveals strong association with RNA splicing and translation machinery. Journal of proteome research. 2010 Feb 5;9(2):1104–20.

35. Colombrita C, Onesto E, Megiorni F, Pizzuti A, Baralle FE, Buratti E, Silani V, Ratti A. TDP-43 and FUS RNA-binding proteins bind distinct sets of cytoplasmic messenger RNAs and differently regulate their post-transcriptional fate in motoneuron-like cells. Journal of Biological Chemistry. 2012 May 4;287(19):15635–47.

36. Smith SA, Ray D, Cook KB, Mallory MJ, Hughes TR, Lynch KW. Paralogs hnRNP L and hnRNP LL Exhibit Overlapping but Distinct RNA Binding Constraints. PLoS ONE. 2013;8(11):e80701.

37. Crooke ST, Vickers TA, Liang X hai. Phosphorothioate modified oligonucleotide–protein interactions. Nucleic Acids Res. 2020;48(10):5235–53.

38. Buratti E, Baralle FE. Characterization and Functional Implications of the RNA Binding Properties of Nuclear Factor TDP-43, a Novel Splicing Regulator ofCFTR Exon 9*. J Biol Chem. 2001;276(39):36337–43.

39. Tan Q, Yalamanchili HK, Park J, Maio AD, Lu HC, Wan YW, White JJ, Bondar VV, Sayegh LS, Liu X, Gao Y, Sillitoe RV, Orr HT, Liu Z, Zoghbi HY. Extensive cryptic splicing upon loss of RBM17 and TDP43 in neurodegeneration models. Hum Mol Genet. 2016;ddw337.

40. Klim JR, Williams LA, Limone F, Juan IGS, Davis-Dusenbery BN, Mordes DA, Burberry A, Steinbaugh MJ, Gamage KK, Kirchner R, Moccia R, Cassel SH, Chen K, Wainger BJ, Woolf CJ, Eggan K. ALS-implicated protein TDP-43 sustains levels of STMN2, a mediator of motor neuron growth and repair. Nature Neuroscience. 2019 Feb;22(2):167–79.

41. Roczniak-Ferguson A, Ferguson SM. Pleiotropic requirements for human TDP-43 in the regulation of cell and organelle homeostasis. Life Sci Alliance. 2019;2(5):e201900358.

42. Bennett CF. Therapeutic Antisense Oligonucleotides Are Coming of Age. Annu Rev Med. 2019;70(1):307–21.

43. Miura M, Sakaue F, Matsuno H, Morita K, Yoshida A, Hara RI, Nishimura R, Nishida Y, Yokogawa M, Osawa M, Yokota T. TDP-43 N-terminal domain dimerisation or spatial separation by RNA binding decreases its propensity to aggregate. FEBS Lett. 2023;597(12):1667–76.

44. Yang C, Tan W, Whittle C, Qiu L, Cao L, Akbarian S, Xu Z. The C-Terminal TDP-43 Fragments Have a High Aggregation Propensity and Harm Neurons by a Dominant-Negative Mechanism. Plos One. 2010;5(12):e15878.

45. Hayes LR, Duan L, Vidensky S, Kalab P. Nuclear Transport Assays in Permeabilized Mouse Cortical Neurons. J Vis Exp. 2021;(173).

ACKNOWLEDGEMENTS

We thank Svetlanta Vidensky, Lyudmila Mamedova, and Fang Yang for expert technical assistance. Selected graphics were created with BioRender.com. This research was supported by NINDS/NIA R01NS123538, NINDS R03NS127011, the Muscular Dystrophy Association, the Guy McKhann Scholar Award (LH), and a JHU Catalyst Award (LH).

AUTHOR CONTRIBUTIONS

Conceptualization PK, LH; Methodology XZ, TD, PK, LH; Investigation XZ, TD, PK, LH; Formal analysis XZ, PK, LH; Visualization XZ, PK, LH; Writing-original draft XZ, PK, LH; Writing-review & editing XZ, TD, PK, LH; Supervision PK, LH; Funding acquisition PK, LH.

DATA AVAILABILITY STATEMENT

No bioinformatics datasets or original code were generated or analyzed during the current study. All raw data are available from the corresponding authors upon request.

ADDITIONAL INFORMATION

COMPETING INTERESTS

The author(s) declare no competing interests.

FIGURE LEGENDS

Figure 1. GU-rich oligonucleotides bind TDP-43 RRM1,2 with variable multivalency

A. Oligonucleotide sequences tested in this study. For base modifications see **suppl table 1a.**

B. EMSA assays in which 10 pmol oligonucleotide was mixed with 0-40 pmol recombinant RRM1-2 protein, resolved under native conditions, and visualized with SYBR gold nucleic acid stain. Band shifts corresponding to predicted monomers (>), dimers (>>), trimers (>>>), or tetramers (>>>>) are indicated.

C. Left: total bound RNA fraction from EMSA assays in (B), quantified as the sum of all shifted bands divided by the total RNA signal. Right: oligomerized RNA fraction from EMSA assays in (B), quantified as the sum of bands predicted to contain >2 RRM1,2 molecules, divided by the total RNA signal. Mean ± SD is shown for 3-6 independent replicates.

D. BS3-crosslinked RRM1,2-oligonucleotide complexes (10 pmol oligo + 40 pmol protein) analyzed by SDS-PAGE and visualized with silver stain. Bands corresponding to predicted monomers (>), dimers (>>), and tetramers (>>>>) are indicated. Representative of 3 independent replicates.

Figure 2. GU-oligonucleotide binding valency predicts the effect on TDP-43 localization in living cells

A. SAV-647 fluorescence in oligonucleotide-transfected HeLa cells at 5 h. Scale bar = 5 μm.

B. SAV-647 N/C 5 h post-transfection. Mean ± SD of ≥4 biological replicates. NS= not significant, ***$p<0.001$, ****$p<0.0001$ by 2-way ANOVA with Tukey's post-hoc test.

C. TDP-43 immunofluorescence in oligonucleotide-transfected HeLa cells at 5 h. The intensity histogram for each image was independently maximized according to the dimmest and brightest pixels and a pseudo-color LUT was applied. Scale bar = 20 μm.

D. TDP-43 N/C (% untreated) in oligonucleotide-transfected HeLa cells at 5 h. Mean ± SD of ≥8 biological replicates. ***p<0.001, ****p<0.0001 by 2-way ANOVA with Tukey's post-hoc test.

Figure 3. GU16 prevents transcriptional blockade-induced TDP-43 mislocalization

A. TDP-43 immunofluorescence in cells transfected with (GU)16 for 5 h followed by 1 h transcriptional blockade with NVP2 (250 nM). The intensity histogram for each image was independently maximized according to the dimmest and brightest pixels and a pseudo-color LUT was applied. Scale bar = 20 μm.

B. TDP-43 N/C (% untreated) in (GU)16-transfected cells with or without NVP2 treatment. Mean ± SD of 15 biological replicates.

C. Nuclear and cytoplasmic intensity in (GU)16-transfected cells (% untreated), with or without NVP2 treatment. These are the source data used to calculate the N/C ratios in B. Mean ± SD of 15 biological replicates.

D-F. TDP-43 N/C (% untreated) in Clip34nt (D), ('AUG12')2 (E), or (CA)16 (F)-transfected cells with or without NVP2 treatment. Mean ± SD of ≥7 biological replicates.

In B-F, NS= not significant, *p<0.05, **p<0.01, ***p<0.001, ****p<0.0001 by 2-way ANOVA with Tukey's post-hoc test. *Note: -NVP2 data are the same as in figure 2.*

Figure 4. (GU)16 induces the formation of high-molecular weight TDP-43 complexes in transfected cells

A. SAV-RNA pulldowns in biotinylated oligo-transfected cells that were UV crosslinked before lysis and probed with rabbit anti-TDP-43. Results are representative of 3 independent biological replicates.

B-F. N/C ratio of hnRNPA1 (B), hnRNPA2B1 (C), Matrin-3 (D), FUS (E), and hnRNPL (F) in cells transfected with (GU)16 for 5 h followed by 1 h with or without NVP2 treatment. Mean ± SD of ≥4 biological replicates for each protein. NS= not significant, ***p<0.001, ****p<0.0001 by 2-way ANOVA with Tukey's post-hoc test.

Figure 5. TDP-43 binding to GU-oligonucleotides is RRM1,2-dependent

A. $TDP43^{WT}$-V5 and $TDP43^{5FL}$-V5 constructs utilized to generate monoclonal cell lines. NTD = N-terminal domain, NLS = nuclear localization signal, RRM = RNA recognition motif, CTD = C-terminal domain.

B-C. TDP43^{WT}-V5 (B) and TDP43^{5FL}-V5 N/C ratio (C) (% untreated) in cell lines transfected with (GU)16 for 5 h, with or without subsequent NVP2 treatment. Mean ± SD of 4 biological replicates per group.

D. TDP-43 N/C (data from B-C) shown as % non-NVP2-treated cells, to permit comparison of NVP2-induced nuclear exit.

E. SAV-RNA pulldowns from biotinylated oligo-transfected cells that were UV crosslinked before lysis and probed with mouse anti-V5 (left) or rabbit anti-TDP-43 (right). Inset demonstrates ~1.4 kDa separation between V5-tagged and endogenous TDP-43 and the presence (TDP43^{WT}-V5 cells, lanes 1-3) or absence (TDP43^{5FL}-V5 cells, lanes 4-6) of TDP-43 autoregulation.

In B-D, NS= not significant, *p<0.05, ***p<0.001, ****p<0.0001 by 2-way ANOVA with Tukey's post-hoc test.

Figure 6. (GU)16 causes TDP-43 partial loss of function in cryptic exon repression

A. TDP-43 Western blot 24 h-post transfection with scrambled siRNA (siScr) or 12.5-25 nM TDP-43 siRNA (siTDP), compared to a stable TDP-43 CRISPR knockout (KO) cell line. Hsp90 is used as a loading control.

B. RT-PCR of EPB41L4A cryptic exon (<) inclusion in (CA)16 vs. (GU)16-transfected cells at 6, 18, and 24 h post-transfection. Controls for TDP-43 expression level include untreated cells (100%), TDP-43 siRNA-treated cells, 24 h (50%), and TDP-43 CRISPR knockout cells (0%). Representative of ≥ 3 biological replicates.

C. qRT-PCR of EPB41L4A cryptic exon inclusion in (CA)16 vs. (GU)16-transfected cells, normalized to EPB41L4A mRNA. TDP-43 expression controls are as in (A-B).

D. Model: Monovalent (GU)6 releases TDP-43 for passive nuclear efflux, while multivalent (GU)16 forms high molecular weight RNP complexes that restrict TDP-43 passive nuclear efflux. TDP-43 binding to PS-modified oligomers disrupts TDP-43 splicing regulatory function by diverting TDP-43 from endogenous transcripts. Optimization is needed to develop an oligonucleotide to scaffold TDP-43 in the nucleus while still permitting TDP-43 functional dynamics.

Figure 1

a

oligo	bp	sequence	valency	effect on TDP-43 localization
(GU)6	12	GUGUGUGUGUGU	single[25]	nuclear exit[21]
'AUG12'	12	GUGUGAAUGAAU	single[9]	nuclear exit[21]
(GU)16	32	GUGUGUGUGUGUGUGUGUGUGUGUGUGUGUGU	*this study*	
Clip34nt	34	GAGAGAGCGCGUGCAGAGACUUGGUGGUGCAUAA		
('AUG12')2	24	GUGUGAAUGAAUGUGUGAAUGAAU		

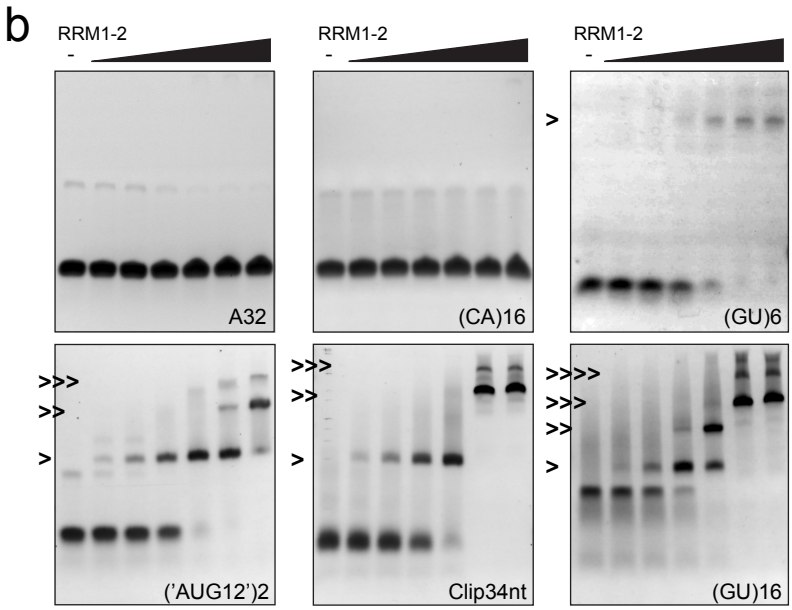

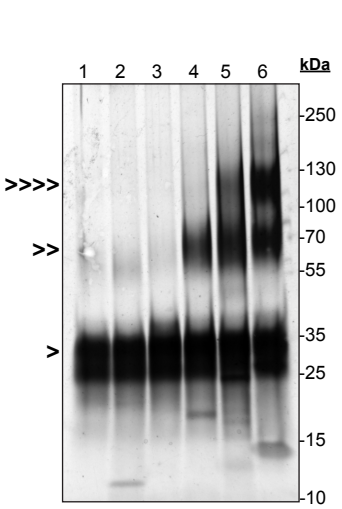

1. RRM1,2-only
2. RRM1,2 + (CA)16
3. RRM1,2 + (GU)6
4. RRM1,2 + ('AUG12')2
5. RRM1,2 + Clip34nt
6. RRM1,2 + (GU)16

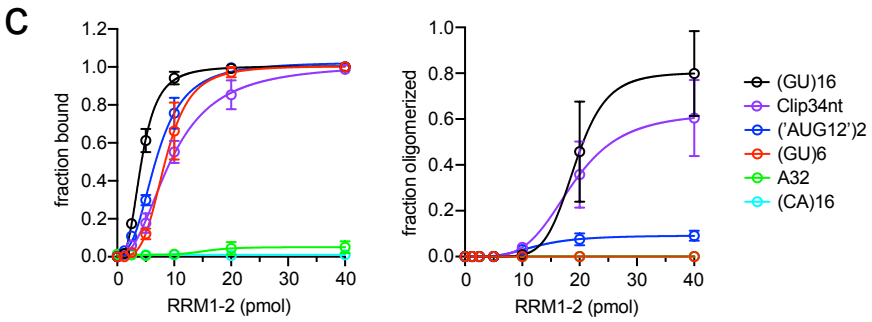

Figure 2

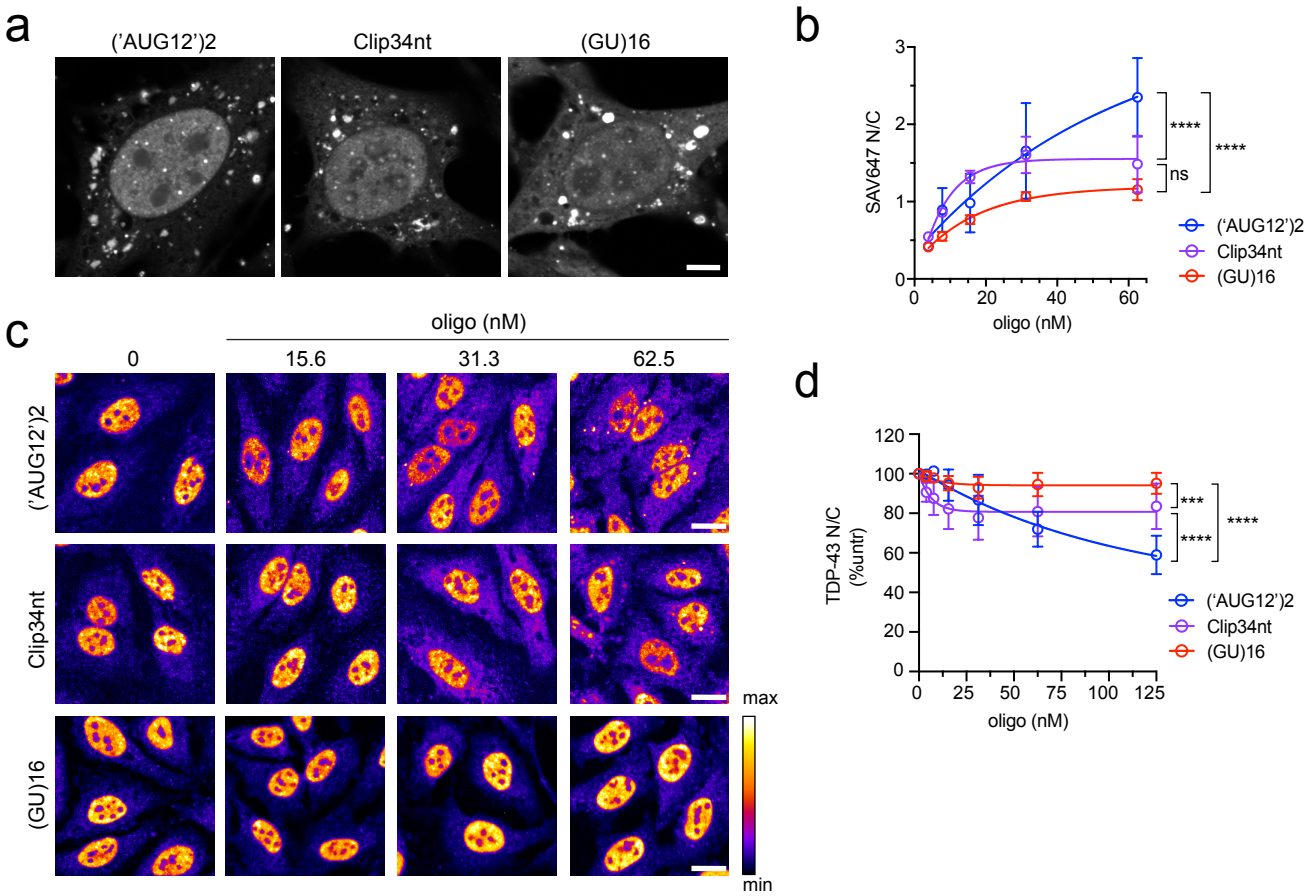
a
('AUG12')2
Clip34nt
(GU)16
b
SAV647 N/C
oligo (nM)
****
****
ns
('AUG12')2
Clip34nt
(GU)16
c
oligo (nM)
0
15.6
31.3
62.5
('AUG12')2
Clip34nt
(GU)16
max
min
d
TDP-43 N/C (%untr)
oligo (nM)
***
****
****
('AUG12')2
Clip34nt
(GU)16

Figure 3

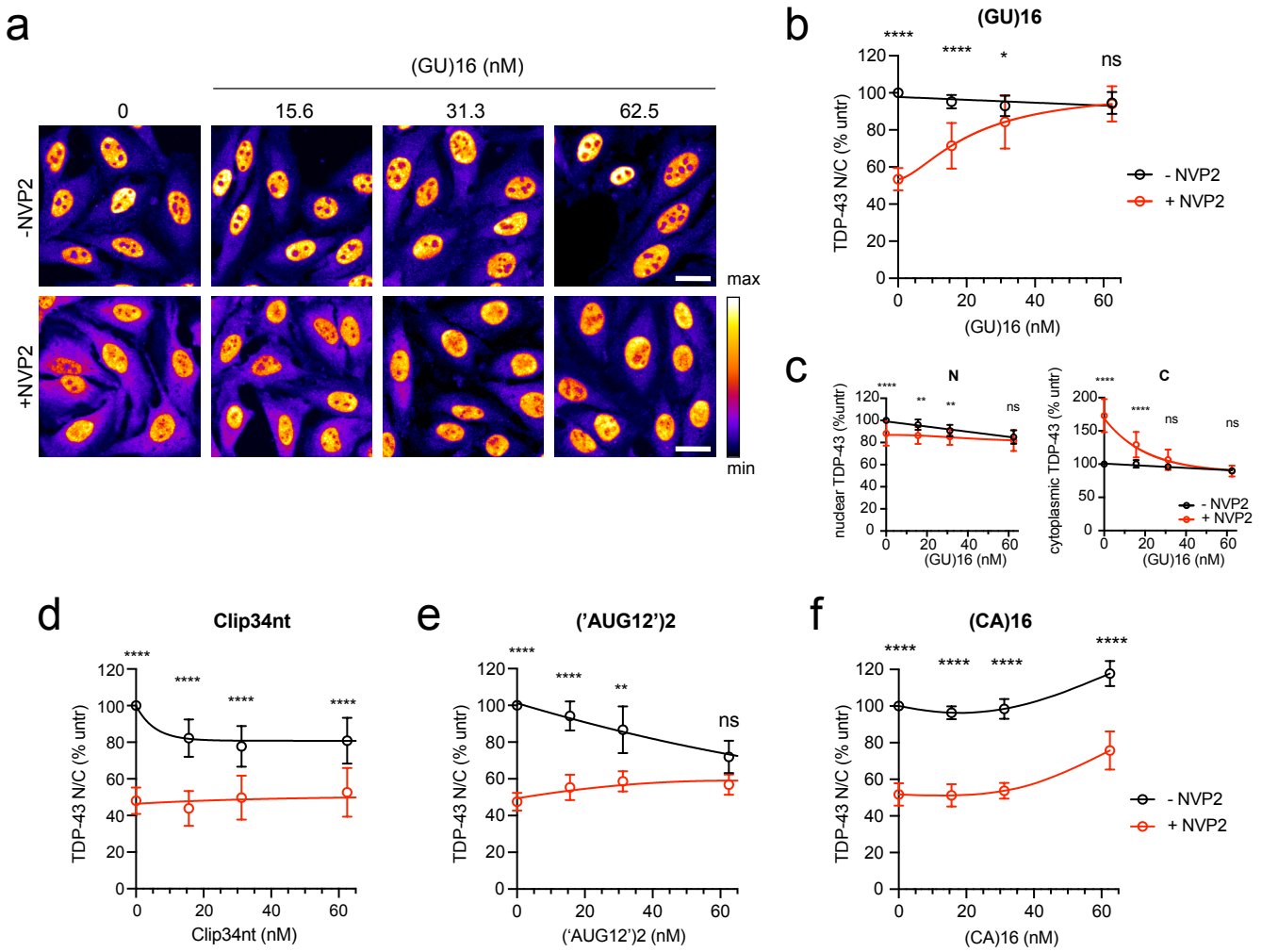
a
(GU)16 (nM)
0
15.6
31.3
62.5
-NVP2
+NVP2
max
min
b
(GU)16
TDP-43 N/C (% untr)
(GU)16 (nM)
- NVP2
+ NVP2
c
N
C
nuclear TDP-43 (%untr)
cytoplasmic TDP-43 (% untr)
(GU)16 (nM)
d
Clip34nt
TDP-43 N/C (% untr)
Clip34nt (nM)
e
('AUG12')2
('AUG12')2 (nM)
f
(CA)16
(CA)16 (nM)

Figure 4

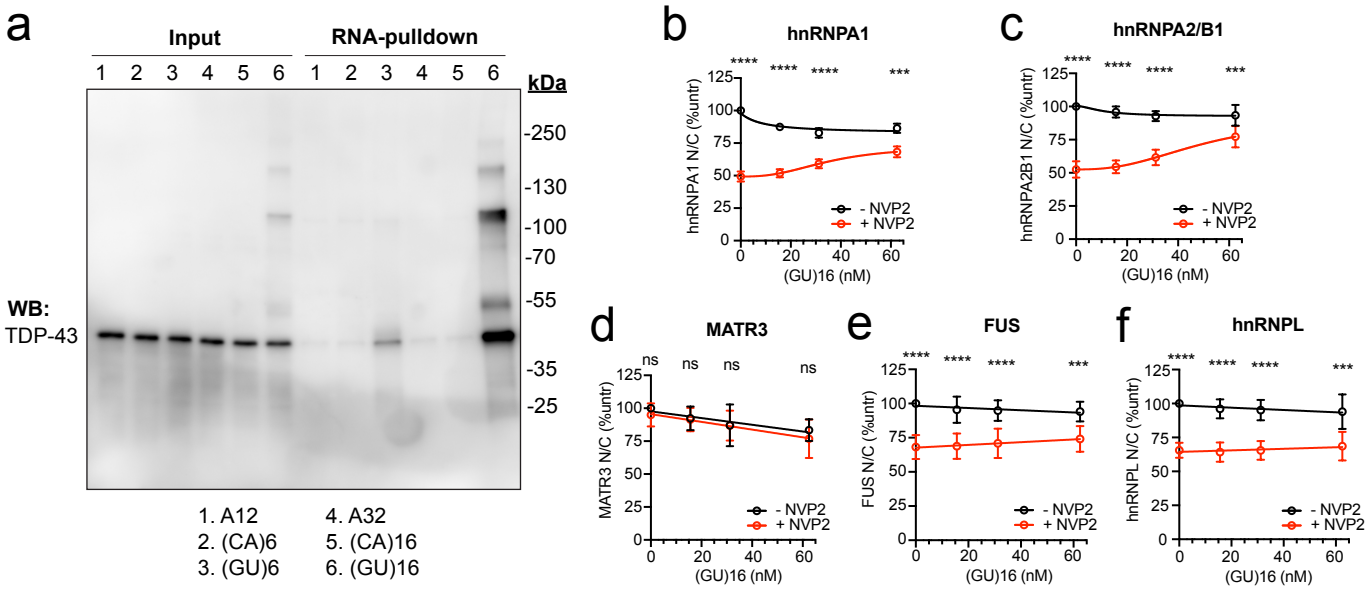
a
Input
RNA-pulldown
1 2 3 4 5 6 1 2 3 4 5 6
kDa
-250
-130
-100
-70
-55
-35
-25
WB:
TDP-43
1. A12
2. (CA)6
3. (GU)6
4. A32
5. (CA)16
6. (GU)16
b
hnRNPA1
hnRNPA1 N/C (%untr)
c
hnRNPA2/B1
hnRNPA2B1 N/C (%untr)
d
MATR3
MATR3 N/C (%untr)
e
FUS
FUS N/C (%untr)
f
hnRNPL
hnRNPL N/C (%untr)
- NVP2
+ NVP2
(GU)16 (nM)

Figure 5

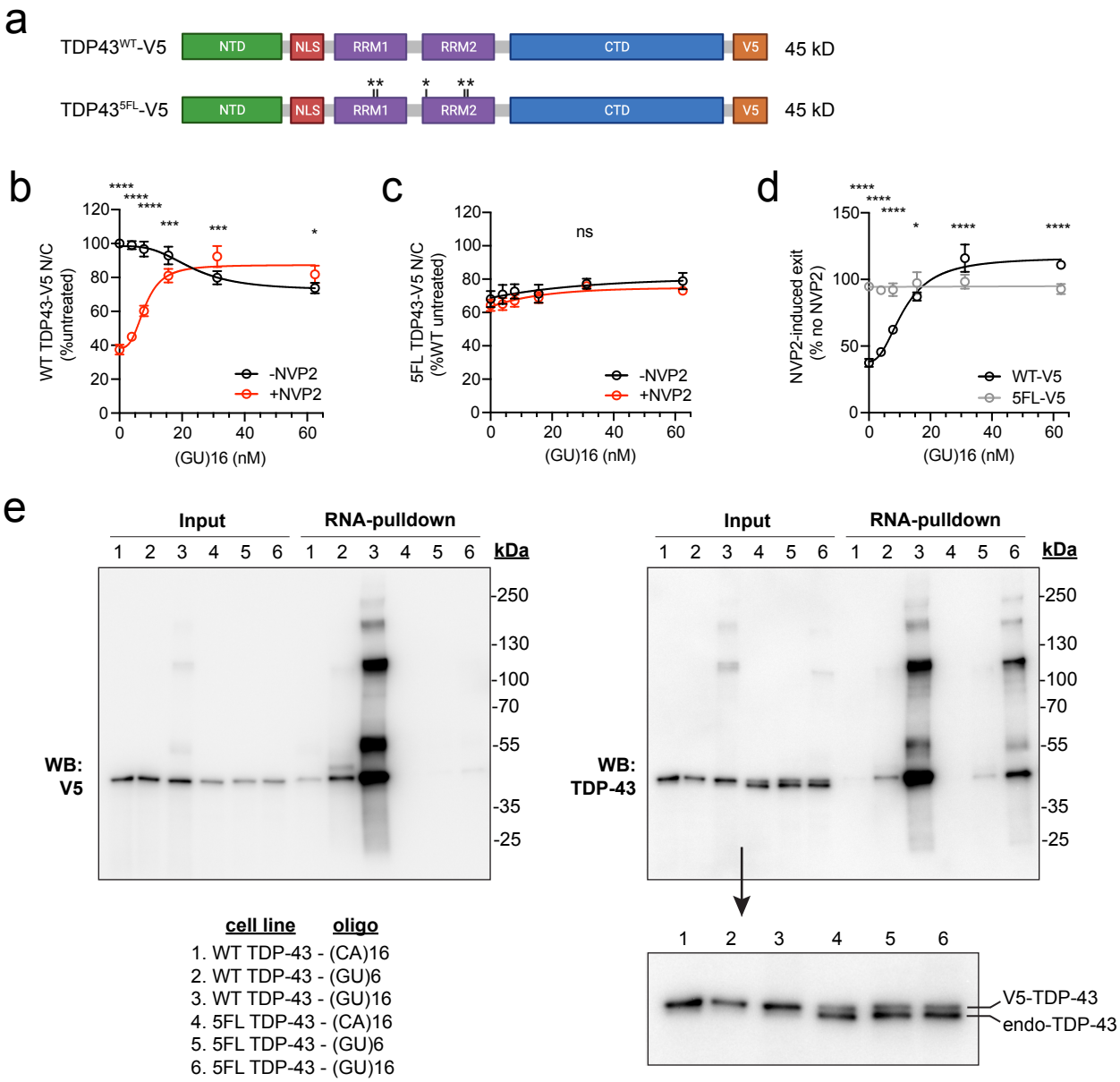
a
TDP43WT-V5
NTD
NLS
RRM1
RRM2
CTD
V5
45 kD
TDP435FL-V5
**
*
**
45 kD
b
WT TDP43-V5 N/C (%untreated)
-NVP2
+NVP2
(GU)16 (nM)
c
5FL TDP43-V5 N/C (%WT untreated)
ns
-NVP2
+NVP2
(GU)16 (nM)
d
NVP2-induced exit (% no NVP2)
WT-V5
5FL-V5
(GU)16 (nM)
e
Input
RNA-pulldown
kDa
WB: V5
WB: TDP-43
cell line oligo
1. WT TDP-43 - (CA)16
2. WT TDP-43 - (GU)6
3. WT TDP-43 - (GU)16
4. 5FL TDP-43 - (CA)16
5. 5FL TDP-43 - (GU)6
6. 5FL TDP-43 - (GU)16
V5-TDP-43
endo-TDP-43

Figure 6

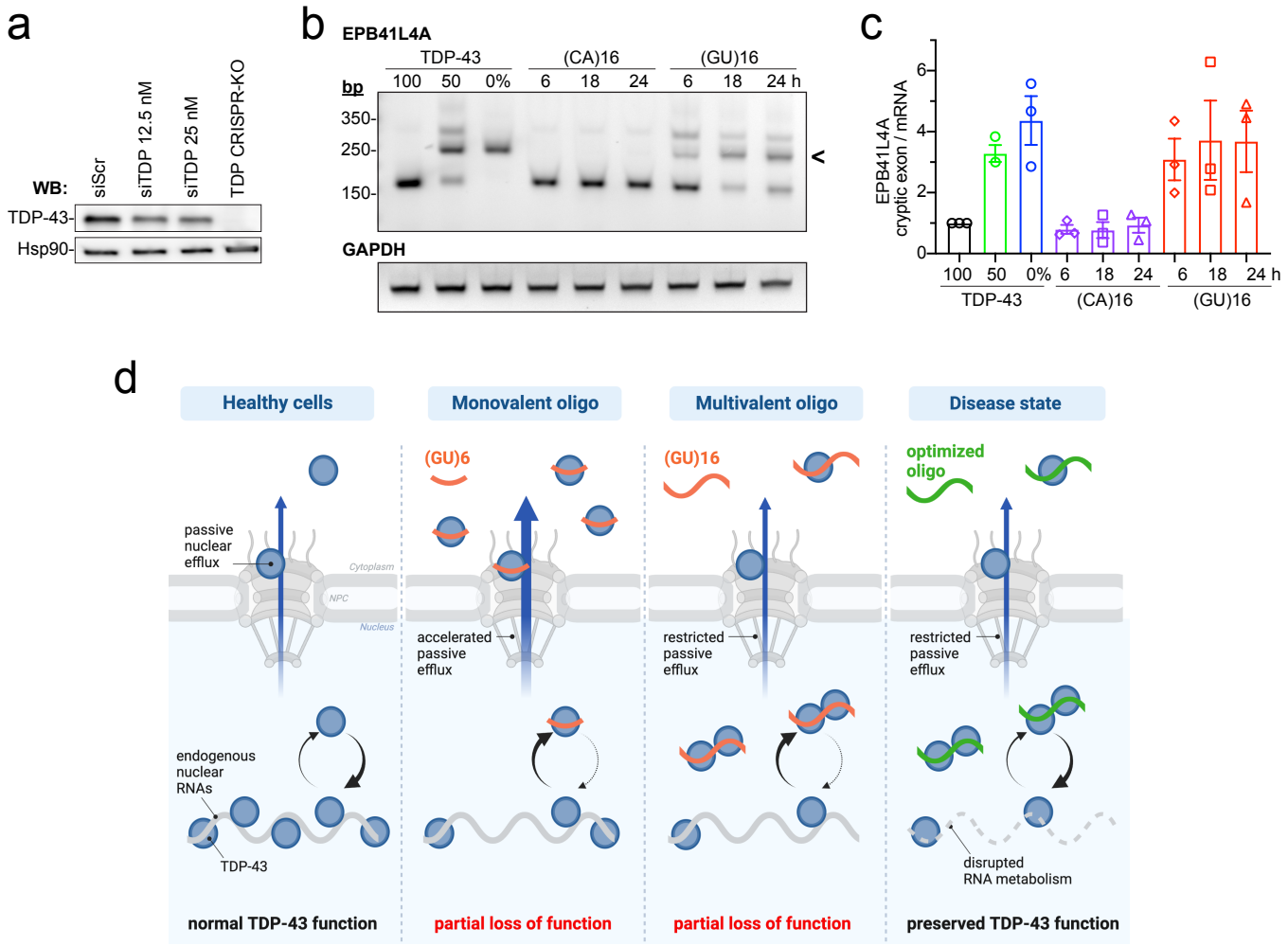
a
WB:
siScr
siTDP 12.5 nM
siTDP 25 nM
TDP CRISPR-KO
TDP-43-
Hsp90-
b
EPB41L4A
TDP-43
(CA)16
(GU)16
bp
100 50 0% 6 18 24 6 18 24 h
350-
250-
150-
GAPDH
c
EPB41L4A
cryptic exon / mRNA
0
2
4
6
100 50 0% 6 18 24 6 18 24 h
TDP-43
(CA)16
(GU)16
d
Healthy cells
Monovalent oligo
Multivalent oligo
Disease state
passive
nuclear
efflux
Cytoplasm
NPC
Nucleus
(GU)6
accelerated
passive
efflux
(GU)16
restricted
passive
efflux
optimized
oligo
restricted
passive
efflux
endogenous
nuclear
RNAs
TDP-43
disrupted
RNA metabolism
normal TDP-43 function
partial loss of function
partial loss of function
preserved TDP-43 function